Iğdır Üniversitesi Fen Bilimleri Enstitüsü Dergisi, 14(2), 755-772, 2024
Journal of the Institute of Science and Technology, 14(2), 755-772, 2024

ISSN: 2146-0574, eISSN: 2536-4618

İnşaat Mühendisliği / *Civil Engineering* **DOI: 10.21597/jist.1405089**

Araştırma Makalesi / *Research Article*

Geliş tarihi / *Received*: 14.12.2023 **Kabul tarihi / *Accepted*: 01.02.2024**

Atıf İçin: Turan, A. I., Ayaz, Y., Yalciner, H., Kumbasaroglu, A. ve Celik, A. (2024). Hızlandırılmış Korozyon Yöntemiyle Paslandırılan Betonarme Çerçeve Sistemlerinin Moment-Taşıma Kapasitelerinin Deneysel ve Analitik İncelenmesi. *Iğdır Üniversitesi Fen Bilimleri Enstitüsü Dergisi*, 14(2), 755-772.

To Cite: Turan, A. I., Ayaz, Y., Yalciner, H., Kumbasaroglu, A. & Celik, A. (2024). Experimental and Analytical Investigation of Moment-Carrying Capacities of Reinforced Concrete Frame Systems Corroded by Accelerated Corrosion Method. *Journal of the Institute of Science and Technology*, 14(2), 755-772.

Hızlandırılmış Korozyon Yöntemiyle Paslandırılan Betonarme Çerçeve Sistemlerinin Moment-Taşıma Kapasitelerinin Deneysel ve Analitik İncelenmesi

Ahmet İhsan TURAN[1*], Yaşar AYAZ[2], Hakan YALÇINER[1], Atila KUMBASAROĞLU[1], Alper ÇELİK[1]

Öne Çıkanlar:
- Korozyon enerji tüketme kapasitesini azaltmaktadır
- Donatı korozyonu moment kapasitesini azaltmaktadır
- Kesit analizi moment değerlerini yüksek oranda tahmin edebilmektedir

Anahtar Kelimeler:
- Korozyon
- Kesit analizi
- Betonarme çerçeve
- Çevrimsel yükleme
- Moment-eğrilik ilişkisi

ÖZET:

Türkiye'de son 25 yılda yaşanan yıkıcı depremlerin ardından yapılan teknik incelemeler, betonarme yapılarda meydana gelen hasarların ana sebeplerinden birinin de donatı korozyonu olduğunu vurgulamaktadır. Donatı korozyonunun betonarme elemanlarda meydana getirdiği bozulmalar, yapının performans seviyesini tanımlayan süneklik, rijitlik, aderans-donatı sıyrılması ilişkisi, taşıma gücü ve enerji yutma kapasitesi gibi parametrelerin azalmasına sebep olmaktadır. Bu bağlamda olası bir sismik hareketlilik yaşanmadan korozyona maruz kalmış betonarme yapıların belirtilen bu performans seviyelerinin tespit edilmesi can ve mal kayıplarının önüne geçilmesi açısından büyük öneme sahiptir. Betonarme yapılarda taşıyıcı eleman davranışını, kesit davranışı yansıtmaktadır. Kesit davranışının doğru bir şekilde tespit edilebilmesi için de Moment-Eğrilik ilişkisinin tanımlanması gerekmektedir. Gerçekleştirilen çalışma ile birlikte korozyona maruz bırakılmış betonarme çerçevelerin yapısal davranışları deneysel ve analitik olarak incelenmiştir. Bu kapsamda üretilen 5 adet betonarme çerçeve numunesinden 4 adedi hızlandırılmış korozyon yöntemiyle farklı oranlarda paslandırılmıştır. Korozyon sürecinin tamamlanmasının ardından, çalışmanın deneysel bölümünde tüm numuneler %20 eksenel ve tersinir-tekrarlanır yanal yük altında deneye tabi tutulmuştur. Analitik çalışmada, korozyon etkisiyle değişen malzeme-mekanik özellikleri dikkate alınarak gerçekleştirilen kesit analizleri sonucunda, hesap edilen moment değerlerinin deneysel olarak ölçülen moment değerleriyle yüksek oranda uyum gösterdiği tespit edilmiştir.

Experimental and Analytical Investigation of Moment-Carrying Capacities of Reinforced Concrete Frame Systems Corroded by Accelerated Corrosion Method

Highlights:
- Corrosion reduces the energy absorption capacity
- Reinforcement bar corrosion reduces moment capacity
- Section analysis can predict moment values to a high degree

Keywords:
- Corrosion
- Section analysis
- Rc frames
- Cyclic load
- Moment-curvature relationship

ABSTRACT:

Technical investigations carried out after the devastating earthquakes in Turkey in the last 25 years show that one of the main causes of damage to reinforced concrete structures is reinforcement bar corrosion. The deterioration caused by reinforcement corrosion in reinforced concrete elements reduces the parameters that define the performance level of the structure, such as ductility, stiffness, bond-slip relationship, load carrying capacity, and energy absorption capacity. Therefore, determining the specified performance levels of reinforced concrete structures exposed to corrosion before any seismic activity occurs is of great importance in preventing loss of life and property. Cross-section behavior in reinforced concrete structures represents the load-bearing element behavior In order to accurately determine the section behavior, the Moment-Curvature relationship must be defined. In this study, the structural behavior of reinforced concrete frames exposed to corrosion was examined experimentally and analytically. For this purpose, 4 of the 5 reinforced concrete frame specimens constructed were corroded at different ratios using the accelerated corrosion method. After the corrosion process was completed, in the experimental part of the study, all specimens were tested under the effect of a 20% constant axial load and reversal-cyclic loading. In the analytical study, as a result of the cross-sectional analyzes carried out by taking into account the material-mechanical properties changing with the effect of corrosion, it was determined that the calculated moment values were in high predicted with the experimentally measured moment values.

[1]Ahmet İhsan TURAN (**Orcid ID:** 0000-0003-4865-6490), Hakan YALÇINER (**Orcid ID:** 0000-0002-7289-3384), Atila KUMBASAROĞLU (**Orcid ID:** 0000-0002-6338-4553), Alper ÇELİK (**Orcid ID:** 0000-0003-3816-680X). Erzincan Binali Yıldırım University, Faculty of Engineering and Architecture, Department of Civil Engineering, Erzincan, Türkiye
[2] Yaşar AYAZ (**Orcid ID:** 0000-0002-1089-0700), İnönü University, Faculty of Engineering, Department of Civil Engineering, Malatya, Türkiye

***Sorumlu Yazar/*Corresponding Author**: Ahmet İhsan TURAN, e-mail: ahmet.turan@erzincan.edu.tr

This study was produced from Ahmet İhsan Turan's PhD thesis.

INTRODUCTION

Earthquakes in Turkey in the last 25 years have caused thousands of deaths and property losses. In the reports and publications performed as a result of instrumental and observational investigations following these devastating earthquakes, the reasons for heavy damage or wholesale collapse of reinforced concrete structures are explained as insufficient concrete compressive strength (Erdik et al., 1992; Tezcan & Ipek, 1996; Lockner et al., 2000; Cagatay et al., 2005; Sengel & Dogan, 2013), reinforcement bar corrosion (Wasti et al., 2001; Kaplan et al., 2004; Binici, 2007; Mondal & Rai, 2008; Akiyama et al., 2013), design errors, workmanship defects, and ground-related situations. In the earthquake regulations that have been developed and entered into force in Turkey since 1975, improvements have been made in the limit values of concrete and reinforcement bar material properties that are allowed to be used in reinforced concrete structures. For example, the lowest compressive strength allowed to be used in reinforced concrete structures is C14 concrete class and C18 concrete class in 1975 ABYYHY (Regulation on Structures to be Built in Disaster Areas) (ABYYHY, 1975), C16 concrete class and C20 concrete class in 1998 ABYYHY (ABYYHY, 1998), and at least C25 concrete class in all structures in TBDY 2018 (Turkish Building Earthquake Regulation) (TBDY, 2018), which is the current regulation whose use has been made mandatory.

Especially considering the structures constructed before 2000, the fact that the regulation requirements remain within certain limits and the use of ready-mixed concrete has not become widespread has made it inevitable for reinforced concrete structures to be constructed with low concrete compressive strength. Reinforcement bar corrosion is commonly seen in reinforced concrete structures with low concrete compressive strength due to permeability problems. Section area losses that occur as a result of reinforcement bar corrosion cause decreases in the bond strength between the reinforcement and concrete. Thus, the structure cause to move away from the performance levels that affect the required boundary conditions under earthquake loads, such as sufficient ductility, sufficient rigidity, and sufficient strength targeted at the design stage (Yalciner et al., 2019; Yalciner et al., 2019; Celik et al., 2020; Yalciner & Kumbasaroglu, 2020; Yalciner et al., 2020; Yalciner & Kumbasaroglu, 2022; Celik et al., 2022). Determining the effects of these parameters, which change as a result of corrosion, on an element and cross-section basis using the moment-curvature relationship obtained from non-linear cross-section analyses is important for determining the performance levels of reinforced concrete structures exposed to corrosion. Considering the current literature, nonlinear section analysis have generally been carried out by taking into account different section types (Caglar et al., 2015; Dok et al., 2017; Cheng et al., 2019), corrosion mechanisms (Zhang et al., 2018), axial load values (Yüksel & Foroughi, 2020), and material properties (Sheikh et al., 2010). For this purpose, in the nonlinear cross-section analyzes carried out in the current research, the deteriorations in the mechanical properties of concrete and reinforcement materials as a result of corrosion effects were calculated with models in the literature and reflected in the analyses. In this context, the XTRACT section analysis program was used to obtain section moment curvature relationships.

MATERIALS AND METHODS

Material and Section Properties

Within the scope of the study, a total of 5 reinforced concrete frame specimens were constructed, including 1 reference with 26 MPa concrete compressive strength and 4 exposed to different ratios of corrosion. The reinforcement and section properties of the test specimens are shown in Figure 1. The column and beam cross-sections of the reinforced concrete frame specimens were dimensioned as 30×30

cm, and the foundation cross-section was dimensioned as 30×40 cm. The net column height of the test specimen, from the upper foundation elevation of the column elements to the lower beam elevation, is 150 cm. The reinforcement cages of the column elements forming the reinforced concrete frames consist of 6 pieces of 14 mm diameter longitudinal reinforcement bar, and the beam elements consist of 5 pieces of 14 mm diameter longitudinal reinforcement bar. Stirrups with an 8 mm reinforcement diameter were placed at 10 cm intervals, and the reinforcement arrangement was produced according to TS-500 (2000). The concrete cover depth used for the RC frames was 30 mm.

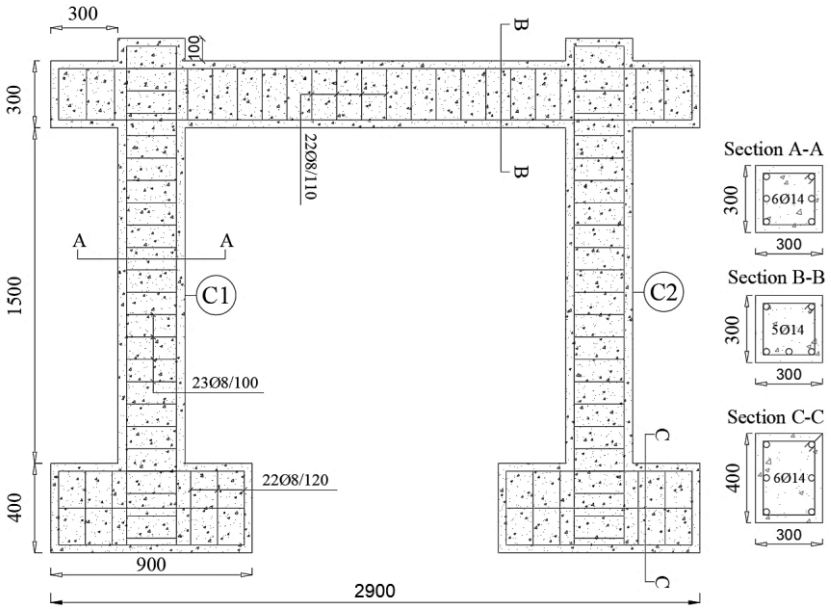

Figure 1. Section properties and detailing of reinforcement bar of the RC frame

Accelerated Corrosion Method

Before the accelerated corrosion process, all longitudinal and stirrups were weighed on a 0.5 g precision scale with a two-point load cell and their initial masses were recorded. Before pouring concrete, as seen in Figure 2, all reinforcements were equipped with 4 mm diameter copper wires in order to ensure a homogeneous current flow in the reinforcements. In order to prevent support problems that may occur due to corrosion of the foundation area of the test sample, the foundation reinforcements were insulated against corrosion. This application aims to prevent deterioration in the mechanical properties of the concrete and reinforcement of the foundation area.

Figure 2. Copper wires used for reinforcement bars (a) Copper wires for longitidunal bars (b) Copper wires used for stirrups, (c) insulation for foundation

For the corrosion tests carried out within the scope of the study, a full-scale reinforced concrete corrosion pool was constructed. Figure 3 shows the front and top view of the corrosion pool.

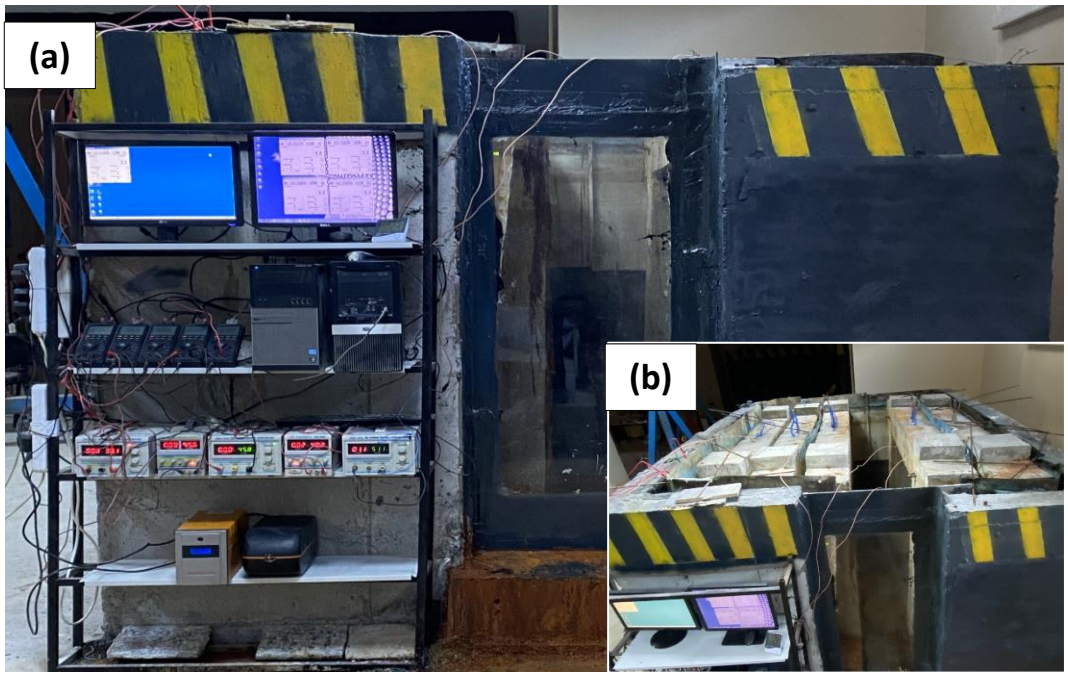

Figure 3. Accelerated corrosion test setup

A power supply with 60 V 0–10 A power, shown in Figure 3, were used to corroded the test specimens. As seen in Figure 3, copper wires extended from the longitudinal reinforcement are connected to the positive terminal of the power supplies to serve as an anode. The cathode circuit element of the accelerated corrosion process is the copper plates surrounding the inner surface of the pool. A digital voltmeter was connected to the system in order to record the current passing through the system in a controlled manner. Faraday's Law, expressed in Equation 1, was used to monitor whether theoretically designed corrosion ratios were reached.

$$mass\ loss = \frac{t(\mathrm{s}) \times I(\mathrm{A}) \times 55.847}{2 \times 96{,}487} \quad (1)$$

Where $t(\mathrm{s})$ is the time and $I(\mathrm{A})$ is the current. The actual corrosion ratio for each specimen was calculated by Eq. (1). As previously mentioned, Faraday's Law has only been used to monitor designed corrosion levels. Actual corrosion levels were obtained by breaking the test specimens after the loading tests, removing all longitudinal bars and stirrups, and reweighing according to Equation 2:

$$C_L = \frac{m_i - m_f}{m_i} \mathrm{x}\ 100 \quad (2)$$

Where m_i, is the original mass of the reinforcement before the corrosion process and m_f , is the mass of the reinforcement after the corrosion products have been removed by the mechanical cleaning process. The average loss in cross-sectional areas of longitudinal reinforcement (ΔA_s) was calculated using Equation 3:

$$\Delta A_s = A_s \times \frac{\Delta_m}{m} \quad (3)$$

Where ΔA_s, is the reinforcement area loss in the cross-section (mm^2), A_s is the cross-sectional area of one non corroded reinforcement bar (mm^2) and Δ_m, is the mass loss per unit length (g/mm) calculated using Equation 4.

$$\Delta m = m - m' \quad (4)$$

Where m and m' are the mass per unit length of non-corroded and corroded reinforcement, respectively (g/mm).

Loading and Measurement Setup

Figure 4 shows the experimental setup designed for corrosion. In reversible lateral cyclic loading experiments, axial loading was applied with two hydraulic pistons with a capacity of 1000 kN fixed on articulated steel plates that were strongly connected to the hard ground with steel bolts. Hydraulic pistons were fixed to the upper steel beam of sufficient length and placed symmetrically on the steel loading beam, welded together at the column ends of the reinforced concrete frame specimen. Thus, axial loading was provided from a single point, with the upper steel beam placed perpendicular to the reinforced concrete frame specimens. The lower loading steel beam placed parallel to the reinforced concrete frame specimens distributed the single load equally to both columns.

As seen in Figure 4, a hydraulic piston with a capacity of 600 kN, fixed to the reaction wall with articulated steel plates, was used for lateral cyclic loading. In order to record the measured values nominally, a 1000 kN load cell was placed by connecting it to the end of the hydraulic piston. Lateral displacements were measured using the LVDT placed on a steel pier anchored to the ground, independent of the specimens at the end of the reinforced concrete frame beam at the applied horizontal load level. In Figure 4, 1- hydraulic piston (600 kN) and load cell (1000 kN) 2- hydraulic piston (1000 kN) 3- steel bolt 4- steel beam 5- anchor to the reaction wall 6-steel bundle 7-reinforced concrete reaction wall 8 - foundation anchor bolts 9- potentiometer (200 mm) 10- represents the test sample.

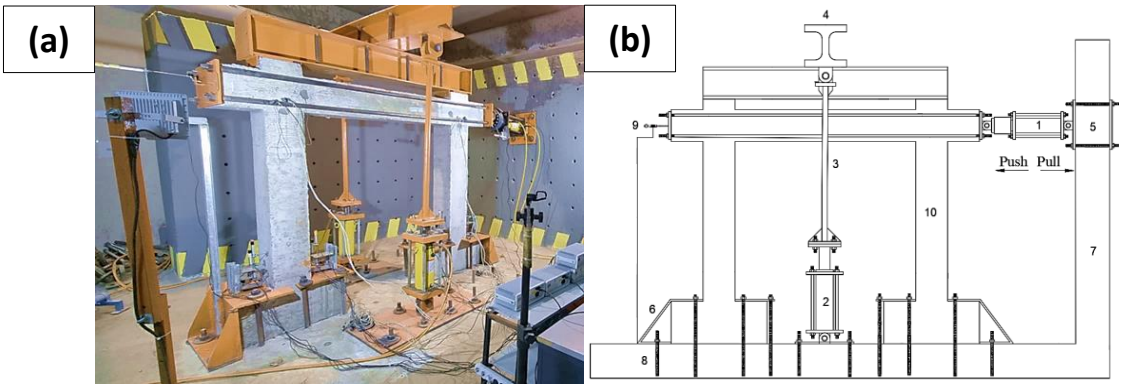

Figure 4. Test setup for loading

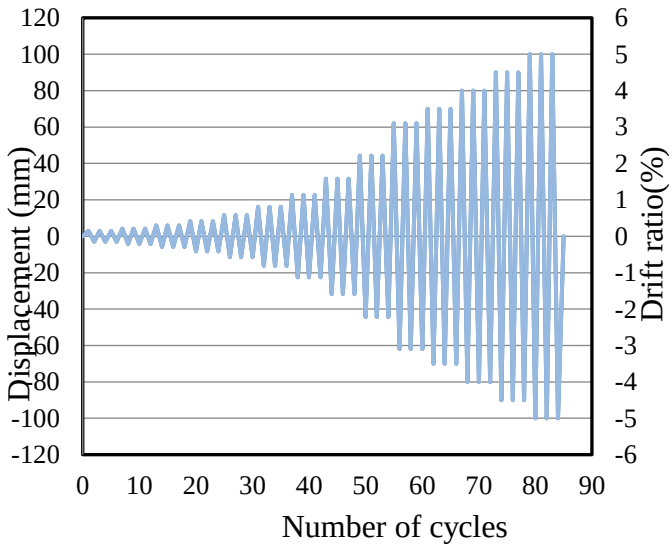

Figure 5 : Loading history program

FEMA 461 (2007) protocol was taken into account in the experiments performed with reversible repetition and displacement control. In the loading protocol considered, 3 cycles were performed for each amplitude. Figure 5 shows the loading history program.

Analytical Study

Concrete model

In the section analyzes carried out within the scope of the analytical study, the stress-strain relationship of confined and unconfined concrete was created according to the concrete model defined in TBEC 2018. Figure 6 shows the parameters taken into account in the confined and unconfined concrete model.

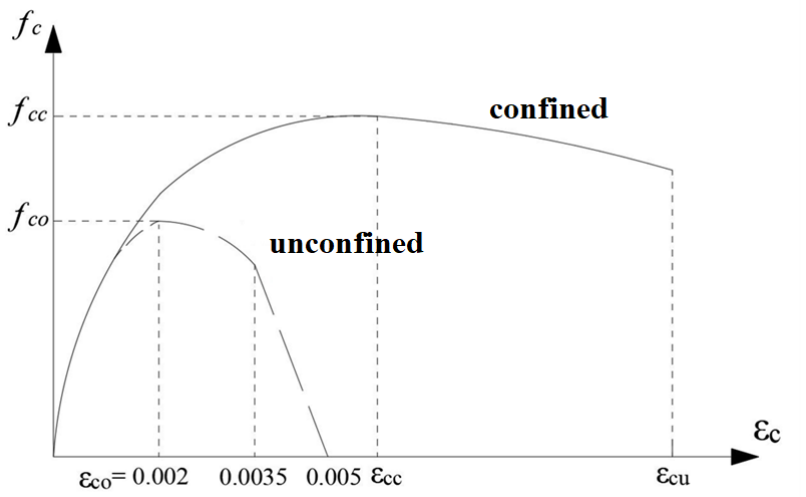

Figure 6 : Stress-strain relationship of the confined and unconfined concretes

The compressive stress in the confined concrete f_c, is calculated as a function of the compressive strain of concrete ε_c by Equation 5.

$$f_c = \frac{f_{cc}\, x\, r}{r\text{-}1+x^r} \tag{5}$$

In Equation 5 f_{cc}, is the confined concrete's strength, x is the strain-dependent variable and r is the elasticity modulus-dependent variable. The relationship between the confined concrete's strength f_{cc} and the unconfined concrete's strength f_{co} is given in Equation 6.

$$f_{cc} = \lambda_c\, f_{co} \tag{6}$$

$$\lambda_c = 2.254 \sqrt{1+7.94 \frac{f_e}{f_{co}}} - 2 \frac{f_e}{f_{co}} - 1.254 \tag{7}$$

In Equation 7, f_e is the effective confining pressure. The effective confining pressure is calculated as the mean of the values given in Equation 8 for two perpendicular directions in rectangular sections.

$$f_{ex} = k_e\, \rho_x f_{yw} \quad , \quad f_{ey} = k_e\, \rho_y f_{yw} \quad , \quad f_e = (f_{ey} + f_{ex})/2 \tag{8}$$

In Equation 8, k_e, is the confining effectiveness coefficient, ρ_x and ρ_y, are the volume fraction of stirrups in the respective directions, and f_{yw}, is the yield strength of the stirrups. The confining effectiveness coefficient k_e is calculated by Equation 9.

$$k_e = \left(1- \frac{\sum a_i^2}{6 b_o h_o}\right)\left(1- \frac{s}{2b_o}\right)\left(1- \frac{s}{2h_o}\right)\left(1- \frac{A_s}{b_o h_o}\right)^{-1} \tag{9}$$

In Equation 9, a_i is the distance between the axes of the vertical reinforcements around the section, b_o and h_o are the section dimensions between the axes of the stirrups confining the core concrete, s is

the stirrup spacing, and A_s is the longitudinal reinforcement area. The relations for the normalized concrete strain x and r in Equation 2 are given in Equation 10 and Equation 11, respectively.

$$x = \frac{\varepsilon_c}{\varepsilon_{cc}} \quad , \quad \varepsilon_{cc} = \varepsilon_{co}[1+5(\lambda_c-1)] \quad , \quad \varepsilon_{co} \approx 0.002 \tag{10}$$

$$r = \frac{E_c}{E_c - E_{sec}} \quad , \quad E_c \approx 5000\sqrt{f_{co}} \quad , \quad E_{sec} = \frac{f_{cc}}{\varepsilon_{cc}} \tag{11}$$

The maximum strain ε_{cu} in the confined concrete is calculated by Equation 12.

$$\varepsilon_{cu} = 0.035 + \frac{1.4\,\rho_s f_{yw}\,\varepsilon_{su}}{f_{cc}} \tag{12}$$

A different approach was adopted in the formation of confined and unconfined concrete models to be used in the analysis of reinforced concrete column sections subjected to corrosion. The reduced compressive strength of the unconfined concrete in the section due to reinforcement corrosion was calculated according to the model proposed by Vecchio and Collins (1986) using the primary corrosion crack widths measured on the reinforced concrete frames (Equation 13).

$$f_c^* = \frac{f_c}{1+K\varepsilon_1/\varepsilon_{co}} \tag{13}$$

In Equation 13, f_c^* is the reduced compressive strength of the unconfined concrete due to corrosion, f_c is the compressive strength of the concrete before corrosion, K is a coefficient dependent on reinforcement diameter and roughness [Cape (1999) suggested 0.1 for deformed reinforced concrete reinforcements], ε_{co} is the strain corresponding to the maximum compressive strength, and ε_1, is the average strain in cracked concrete in the direction perpendicular to the compression direction. ε_1 is calculated by Equation 14.

$$\varepsilon_1 = (b_f - b_o)/b_o \tag{14}$$

In Equation 14, b_o is the section width before corrosion cracking and b_f is the total section width increased due to corrosion cracking. The average strain in cracked concrete ε_1 was calculated using the average primary corrosion crack widths W_{cr} measured on corroded reinforced concrete column specimens in the experimental section of the study. Table 1 shows the average primary corrosion crack widths measured along the height of the reinforced concrete frame specimens.

Decreases in compressive strength due to cracks occurring as a result of corrosion in the unconfined concrete were calculated. Considering the average section losses in the coiled reinforcement due to corrosion, the reinforcement ratios in Equation 4 were calculated for each sample and a confined concrete model was created for reinforced concrete sections exposed to corrosion.

The confined and unconfined concrete models used in for the reinforced concrete column sections subjected to corrosion are shown in Figure 7.

Table 1. Average initial corrosion crack widths

Specimen		CL_L (%)	CL_s (%)	W_{cr} (mm)
RCF1	Left	11.3	4.9	0.28
	Right	12.8	4.1	0.34
RCF2	Left	17.3	4.6	0.37
	Right	14.6	4.1	0.35
RCF3	Left	22.3	12.2	0.44
	Right	20.6	13.1	0.39
RCF4	Left	27.3	20.2	0.58
	Right	23.9	17.4	0.42

CL_L: Corrosion level of the longitudinal reinforcements, **CL_S:** Corrosion level of the stirrups, **W_{cr}:** Crack width (mm)

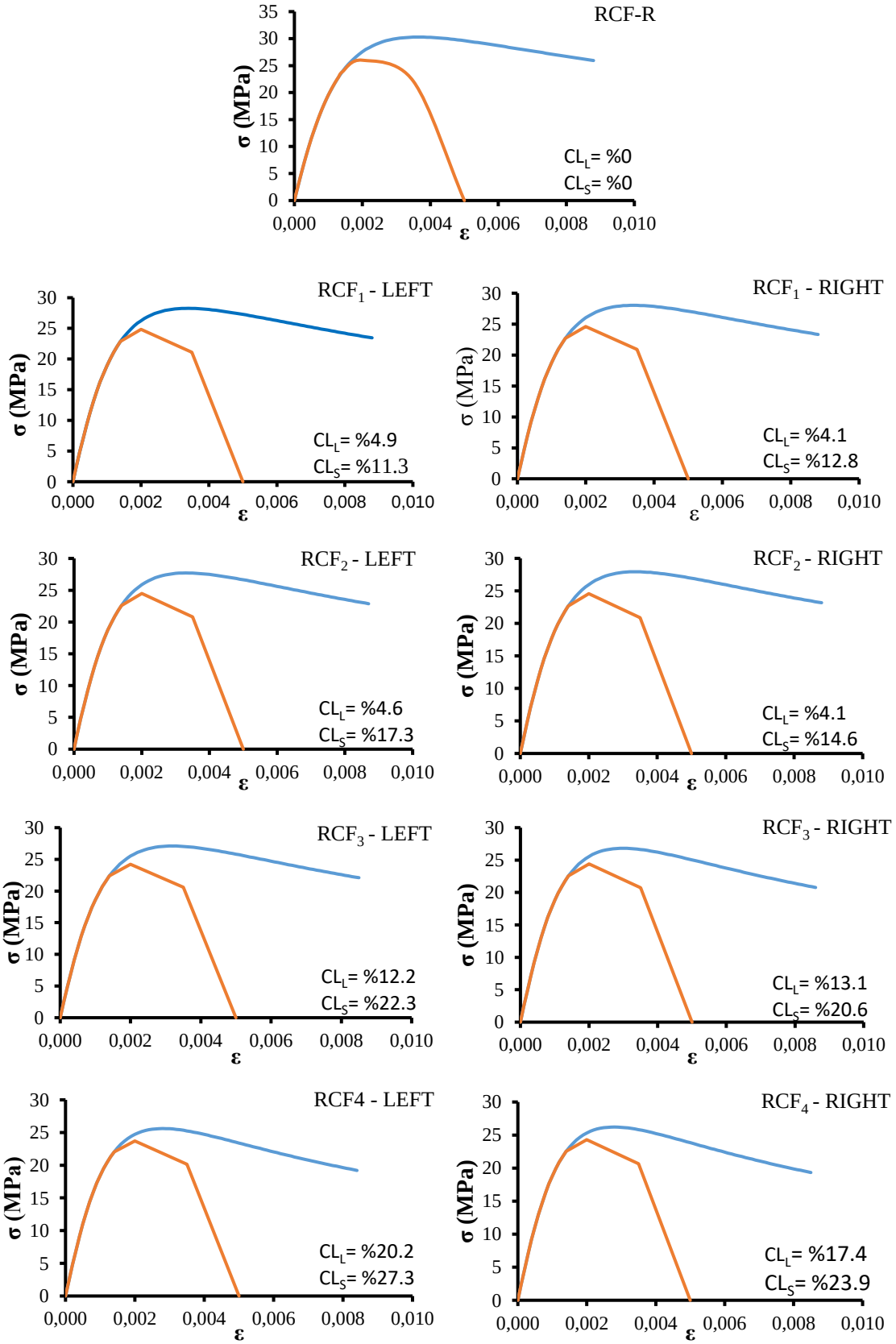

Figure 7. Confined and unconfined corroded concrete models

Reinforcement model

Within the scope of the analytical study, mechanical properties obtained from the tensile test results were used for the reinforcement used in the non-corroded reference specimen RCF_R. Although reinforcement corrosion in reinforced concrete elements generally occurs homogeneously, in some cases it can also be seen as pitting. Pitting corrosion in the reinforcement negatively affects the mechanical properties of the reinforcement and causes premature rupture under flexural and tensile effects. The complexity of estimating section losses resulting from the pitting corrosion mechanism makes it difficult to model them in analytical studies. For this reason, models that take homogeneous corrosion into account were used in the analytical study.

Yield stresses and elasticity module of reinforcement were calculated as a function of the corrosion level using the models developed by Wang and Liu (2008) (Equations 15-16), and ultimate stress and strain values were calculated using the models developed by Wu and Yuan (2008) (Equations 17-18).

$$f_{yc} = (1\text{-}0.0198\delta) f_y \quad (15)$$

$$E_{sc} = (1\text{-}0.0118\delta) E_s \quad (16)$$

$$f_{uc} = (1\text{-}0.0190\delta) f_u \quad (17)$$

$$\varepsilon_{uc} = (1\text{-}0.0210\delta) \varepsilon_u \quad (18)$$

The actual corrosion levels of all reinforcements in the corroded reinforced concrete frame specimens were determined by a gravimetric study. The actual corrosion levels were calculated using the empirical equations above and the changing mechanical properties of each reinforcement were calculated. In line with Turkish Building Earthquake Code (TBEC, 2018), the strain value at which the hardening starts was considered as 1/10 of the ultimate strain value. Tables 3-5 shows the mechanical properties of all reinforcements used in the sections within the scope of the analytical study and the final reinforcement diameter values (D_B) after section loss.

Table 2. Mechanical properties of the reinforcement bars for right column RCF_1 and RCF_2

Specimen		*n*	*CL_L (%)*	*D_B (mm)*	*As*	*ε_y*	*ε_{sh}*	*ε_u*	*f_y (MPa)*	*f_u (MPa)*	*E (MPa)*
RCF-R		1-8	0	14	153.9	0.0022	0.0116	0.116	500	590	227273
Right	RCF-1	1	5.46	13.63	146	0.0021	0.0102	0.102	445.9	528.75	213239
		2	2.14	13.85	150.7	0.0022	0.011	0.11	478.83	566.03	221782
		3	5.96	13.6	145.3	0.0021	0.0101	0.101	440.96	523.15	211957
		4	2.43	13.83	150.3	0.0022	0.011	0.11	475.9	562.71	221021
		5	5.09	13.66	146.5	0.0021	0.0103	0.103	449.62	532.95	214203
		6	4.78	13.68	146.9	0.0021	0.0104	0.104	452.69	536.43	215000
	RCF-2	1	5.1	13.66	146.5	0.0021	0.0103	0.103	449.53	532.85	214180
		2	4.59	13.69	147.2	0.0021	0.0104	0.104	454.55	538.54	215483
		3	2.76	13.81	149.8	0.0021	0.0109	0.109	472.72	559.11	220196
		4	6.25	13.58	144.9	0.0021	0.01	0.1	438.13	519.94	211222
		5	5.27	13.64	146.2	0.0021	0.0103	0.103	447.78	530.87	213727
		6	1.6	13.89	151.5	0.0022	0.0112	0.112	484.16	572.06	223164

Table 3. Mechanical properties of the reinforcement bars for right column RCF_3 and RCF_4

Specimen		*n*	*CL_L (%)*	*D_B (mm)*	*As*	*ε_y*	*ε_{sh}*	*ε_u*	*f_y (MPa)*	*f_u (MPa)*	*E (MPa)*
Right	RCF-3	1	18.52	12.86	129.9	0.0018	0.0071	0.071	316.64	382.38	179708
		2	15.67	13.02	133.1	0.0018	0.0078	0.078	344.9	414.38	187038
		3	9.79	13.36	140.2	0.002	0.0092	0.092	403.13	480.31	202143
		4	19.05	12.83	129.3	0.0017	0.0069	0.069	311.43	376.48	178355
		5	18.88	12.84	129.5	0.0018	0.007	0.07	313.09	378.36	178785
		6	9.33	13.39	140.8	0.002	0.0093	0.093	407.65	485.44	203317

Table 3. Mechanical properties of the reinforcement bars for right column RCF_3 and RCF_4 (continued)

Right	RCF-4	1	23.03	12.62	125.1	0.0016	0.006	0.06	272.03	331.87	168135
		2	15.22	13.04	133.6	0.0019	0.0079	0.079	349.36	419.43	188196
		3	15.62	13.02	133.1	0.0018	0.0078	0.078	345.37	414.91	187159
		4	27.37	12.4	120.9	0.0015	0.0049	0.049	229.04	283.19	156983
		5	21.18	12.72	127	0.0017	0.0064	0.064	290.35	352.61	172888
		6	25.28	12.51	122.9	0.0015	0.0054	0.054	249.7	306.58	162342

Table 4. Mechanical properties of the reinforcement bars for left column RCF_1 and RCF_2

Specimen		***n***	***CL_L (%)***	***D_B (mm)***	***As***	***ε_y***	***ε_{sh}***	***ε_u***	***f_y (MPa)***	***f_u (MPa)***	***E (MPa)***
Left	RCF-1	1	4.41	13.70	147.4	0.0021	0.0105	0.105	456.29	540.51	215935
		2	3.89	13.74	148.2	0.0021	0.0106	0.106	461.50	546.40	217284
		3	6.04	13.60	145.2	0.0021	0.0101	0.101	440.22	522.31	211765
		4	5.59	13.62	145.8	0.0021	0.0102	0.102	444.67	527.35	212920
		5	5.00	13.66	146.6	0.0021	0.0103	0.103	450.45	533.90	214419
		6	6.00	13.60	145.2	0.0021	0.0101	0.101	440.56	522.70	211854
	RCF-2	1	4.53	13.69	147.3	0.0021	0.0105	0.105	455.16	539.23	215641
		2	2.46	13.83	150.2	0.0022	0.0110	0.110	475.68	562.47	220965
		3	4.05	13.72	147.9	0.0021	0.0106	0.106	459.89	544.58	216868
		4	5.85	13.61	145.4	0.0021	0.0101	0.101	442.04	524.38	212238
		5	3.91	13.73	148.1	0.0021	0.0106	0.106	461.32	546.20	217238
		6	8.31	13.45	142.1	0.0020	0.0095	0.095	417.75	496.87	205937

Table 5. Mechanical properties of the reinforcement bars for left column RCF_3 and RCF_4

Specimen		***n***	***CL_L (%)***	***D_B (mm)***	***As***	***ε_y***	***ε_{sh}***	***ε_u***	***f_y (MPa)***	***f_u (MPa)***	***E (MPa)***
Left	RCF-3	1	20.98	12.73	127.2	0.0017	0.0065	0.065	292.34	354.87	173404
		2	6.25	13.58	144.9	0.0021	0.0100	0.100	438.17	519.99	211234
		3	19.62	12.80	128.7	0.0017	0.0068	0.068	305.79	370.09	176892
		4	12.32	13.21	137.1	0.0019	0.0086	0.086	378.02	451.88	195631
		5	13.88	13.12	135.2	0.0019	0.0082	0.082	362.57	434.38	191621
		6	11.38	13.27	138.2	0.0020	0.0088	0.088	387.31	462.40	198041
	RCF-4	1	23.96	12.57	124.2	0.0016	0.0057	0.057	262.75	321.36	165727
		2	21.59	12.70	126.6	0.0017	0.0063	0.063	286.24	347.96	171821
		3	37.76	11.93	111.7	0.0010	0.0024	0.024	126.15	166.68	130291
		4	23.45	12.60	124.7	0.0016	0.0059	0.059	267.88	327.16	167057
		5	16.71	12.96	131.9	0.0018	0.0075	0.075	334.61	402.73	184369
		6	30.54	12.25	117.9	0.0013	0.0041	0.041	197.67	247.66	148844

RESULTS AND DISCUSSION

Actual Corrosion Ratio

In order to determine the actual corrosion rates of reinforced concrete frames, each longitudinal and was removed from the concrete by crushing operations carried out after the reversible cyclic loading tests (Figure 8a). In order to accurately determine the mass loss of the samples after corrosion, all waste concrete and rust products on the reinforcement surface must be cleaned. In this context, first mechanical and then chemical cleaning processes were applied to all reinforcement in accordance with the ASTM G1-03 (2003) standard (Figure 8b). Mechanical cleaning process was carried out with fringed wire brushes and chemical cleaning process was carried out by preparing Clarke solution. After the cleaning process was completed, the final mass values of the reinforcement were obtained using a two-point load cell scale with 0.5 g sensitivity (Figure 8c).

Figure 8. Acquire actual corrosion ratio (a) breaking of concrete (b) chemical cleaning (c) weighing of the all reinforcement bars

Actual corrosion rates of all representative numbered longitudinal and stirrups of corroded reinforced concrete frame samples are given in Figure 9, depending on the calculated (%) mass loss relationship. It is understood from Figure 9 that the corrosion levels of stirrups are considerably higher than the corrosion levels of longitudinal reinforcement. This situation can be attributed to many factors: The simultaneous initiation of the corrosion process in both longitudinal and stirrups bars causes corrosion to begin earlier in the stirrups. The fact that the stirrups are closer to the specimen surfaces facilitates the penetration of chloride ions, oxygen and moisture, leading to more severe corrosion and wider concrete transverse cracks. For a constant depth of reinforcement corrosion, a larger reinforcement diameter corresponds to a lower measured corrosion ratio.

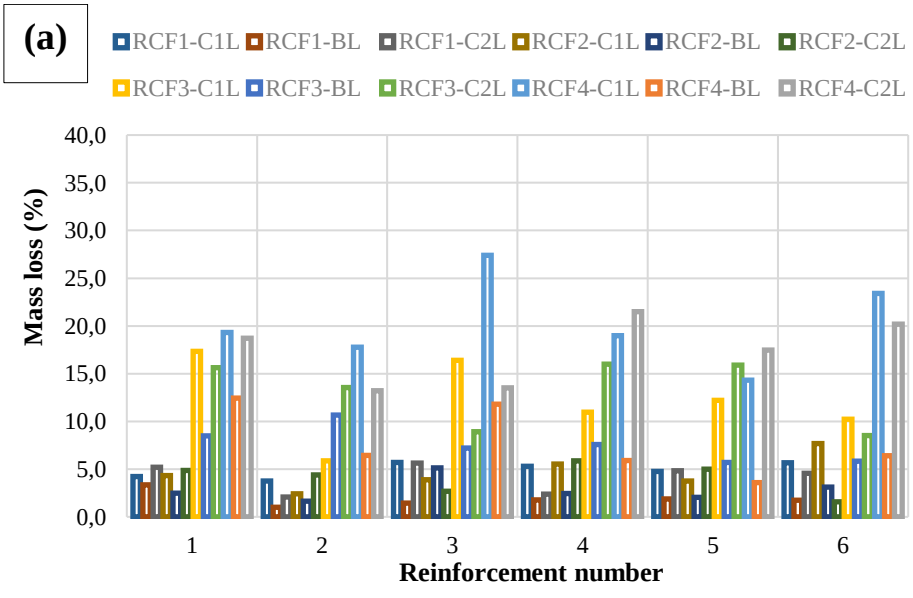

Figure 9. Actual corrosion ratio (a) longitudinal reinforcement bars (b) stirrups bars

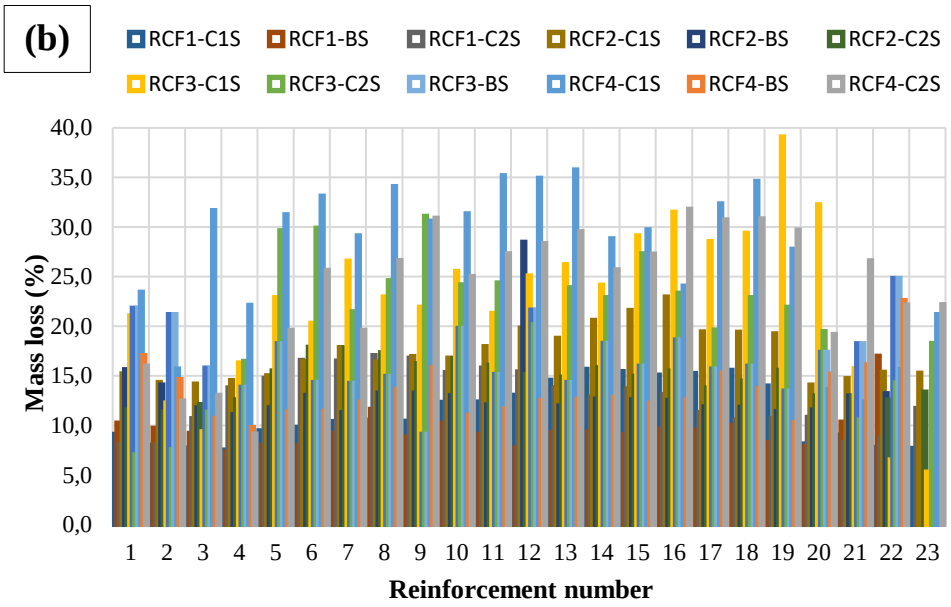

Figure 9. Actual corrosion ratio (a) longitudinal reinforcement bars (b) stirrups bars (continued)

Load-Displacement Relationships

Loading tests of reinforced concrete frames were carried out under the influence of cyclic loading and constant 20% axial load ($N_d = 0.2(A_c \times f_{ck})$. Lateral load values were obtained with the load cell placed at the end of the hydraulic piston, and the displacements obtained in the cycles were obtained with the potentiometer placed at the midpoint of the beam, and load-displacement graphs were created for all test samples. The drift ratio was defined by measuring the distance from the midpoint of the beam to the top of the foundation beam. The cyclic envelope curves defining the load-displacement capacity limit are shown in Figure 10.

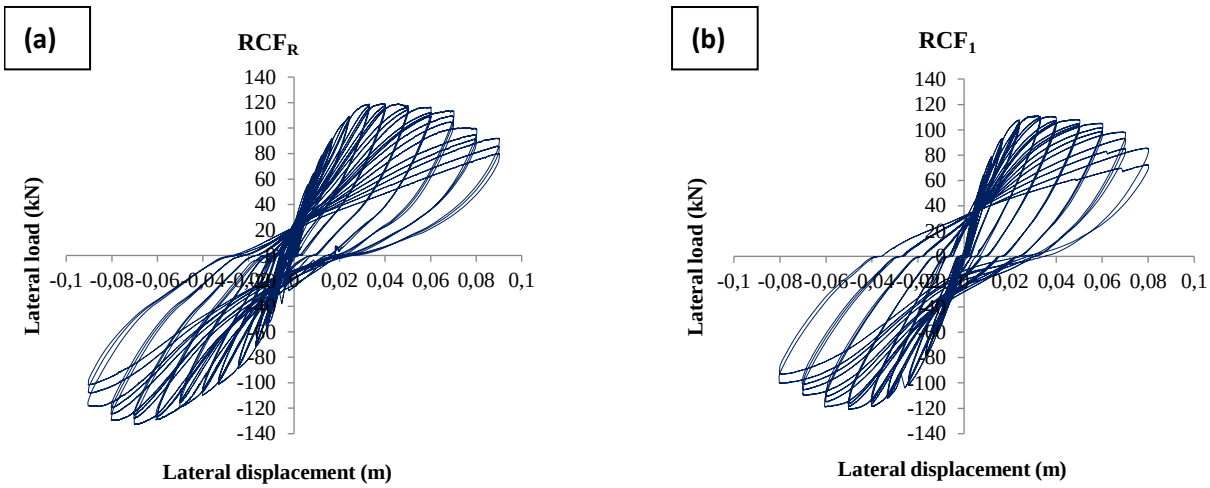

Figure 10. Hysteretic loops: (a) RCFR; (b) RCF1; (c) RCF2; (d) RCF3; (e) RCF4

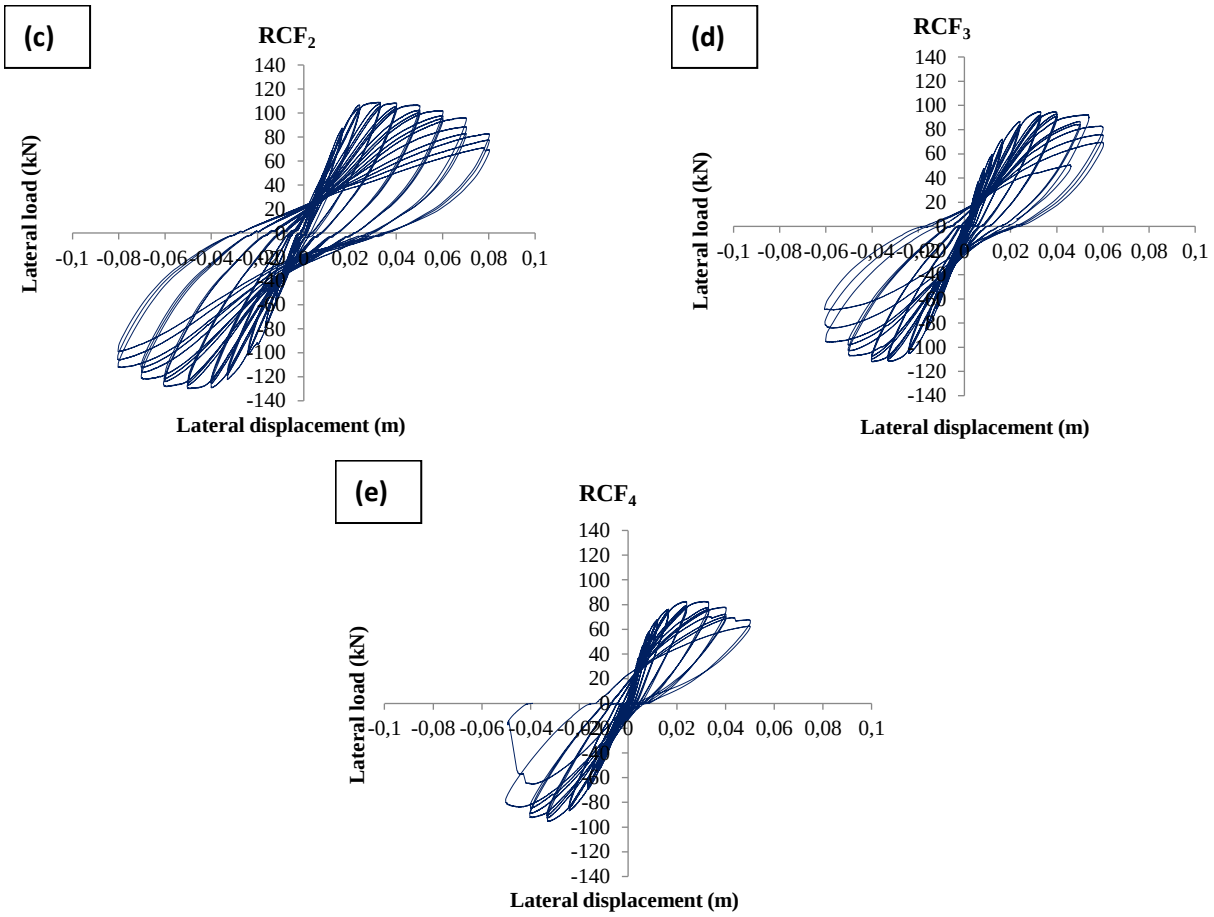

Figure 10. Hysteretic loops: (a) RCF_R; (b) RCF_1; (c) RCF_2; (d) RCF_3; (e) RCF_4 (continued)

As a result of the examination of the load-displacement graphs, it is seen that the number of cycles decreases as the corrosion rate increases. This is due to the fact that samples that reach early yielding state reach their bearing capacity at lower displacement values and have less energy absorption capacity. For example, the yield load and energy absorption capacity of the RCF_4 specimen, which had the highest average corrosion rate among the test samples with 17.11%, decreased by 25% and 71%, respectively, when the reference specimen was taken into consideration. The measured relative mechanical properties and moment-carrying capacities of each experimental specimen are summarized in Table 5 and 7 respectively.

Analytical results of the research

Section analysis were carried out to examine the effect of corrosion in reinforced concrete reinforcement bars on reinforced concrete sections under the influence of axial load and bending moment. In cross-section analyses, the negatory effects of reinforcement corrosion on concrete compressive strength and confinement effect were taken into account in concrete models with the help of empirical relations. The changing mechanical properties of rusted reinforced concrete reinforcements were also calculated with empirical relations and were reflected in the cross-sectional analyzes together with the diameter values calculated depending on the section losses. The moment-curvature relationships and the bending moment-axial load curves of the obtained from the sectional analyzes carried out with the effect of 20% axial load are shown in Figs. 11-12 respectively. In addition the moment-curvature relationship results are summarized in Table 6.

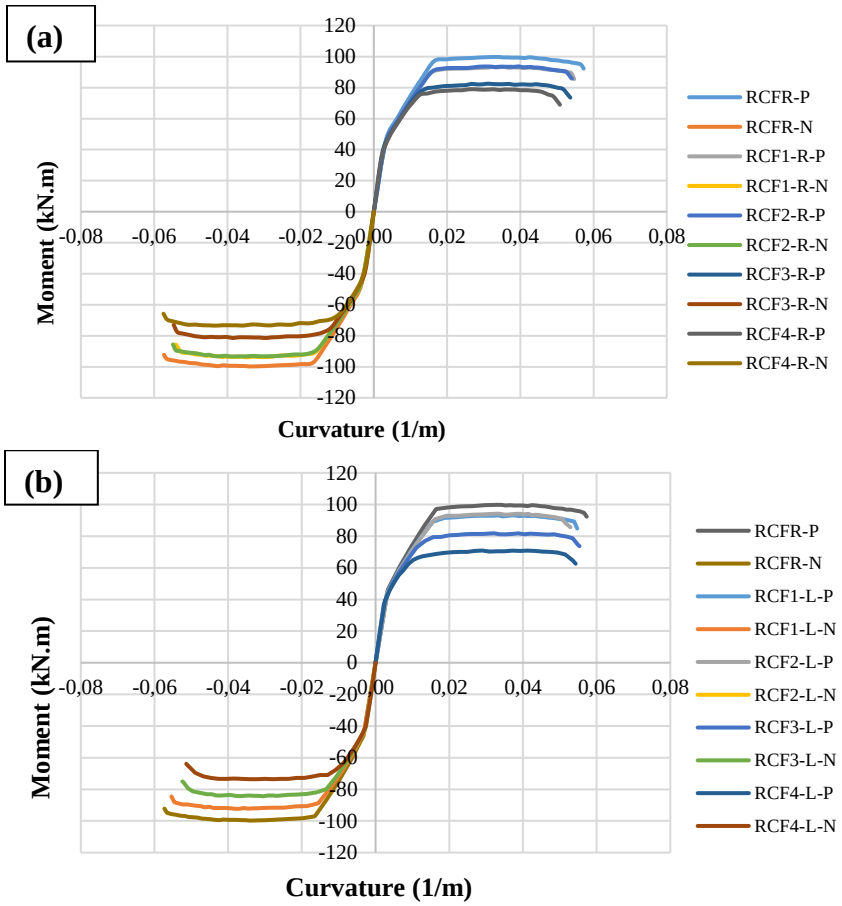

Figure 11. Moment-curvature relationships: (a) Left columns, (b) Right colums

In Fig. 12, the line of $0.4A_cf_{ck}$ represents the maximum allowable load that can be carried by a section according to the Turkish Building Earthquake Code (TBEC, 2018), where A_c is the cross-sectional area of a section. On the limit state line of $0.4A_cf_{ck}$, the moment capacity of the corroded RC section decreases as a function of corrosion level. The moment capacity of the non-corroded frame is 122 kN-m on this line, but this capacity decreased to 112 kN.m, 109 kN.m, 102 kN.m, and 94 kN.m after RCF_1, RCF_2, RCF_3, and RCF_4 specimens, respectively.

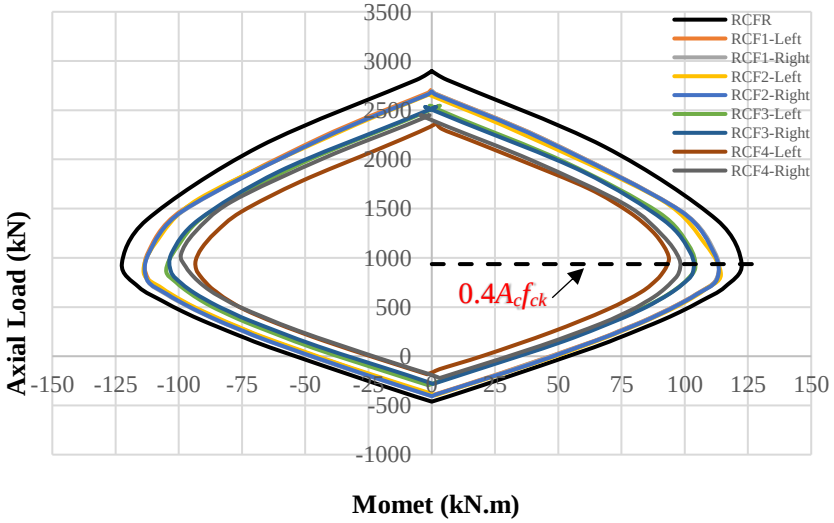

Figure 12. The bending moment-axial load interaction diagrams

Table 6. Moment-curvature results calculated from analytical study

Specimens		Loading direction	M_y (kN.m)	$Ø_y$ (1/m)	M_u (kN.m)	$Ø_u$ (1/m)	$\mu_ø$	E (kN-m)
Right	RCF-R	P						
		N	97.13	0.020	92.25	0.057	2.90	5.06
		O						
	RCF-1	P	88.90	0.019	85.65	0.055	2.86	4.52
		N	89.81	0.019	85.83	0.054	2.79	4.50
		O	89.36	0.019	85.74	0.054	2.82	4.51
	RCF-2	P	89.90	0.020	85.69	0.054	2.76	3.95
		N	89.01	0.019	85.51	0.054	2.82	4.48
		O	89.46	0.019	85.60	0.054	2.79	4.22
	RCF-3	P	75.56	0.015	73.68	0.054	3.56	3.99
		N	74.99	0.015	72.82	0.055	3.71	4.03
		O	75.28	0.015	73.25	0.054	3.63	4.01
	RCF-4	P	70.19	0.014	68.98	0.051	3.68	3.61
		N	65.57	0.012	65.78	0.057	4.93	3.88
		O	67.88	0.013	67.38	0.054	4.30	3.75
Left	RCF-1	P	88.88	0.019	84.91	0.054	2.82	4.50
		N	88.91	0.019	84.09	0.055	2.88	4.50
		O	88.90	0.019	84.50	0.05	2.85	4.50
	RCF-2	P	90.78	0.020	86.63	0.053	2.64	4.37
		N	86.99	0.018	83.88	0.056	3.04	4.55
		O	88.89	0.019	85.26	0.05	2.84	4.46
	RCF-3	P	72.83	0.014	73.71	0.055	3.88	4.09
		N	79.80	0.017	75.01	0.052	3.11	3.96
		O	76.32	0.015	74.36	0.05	3.49	4.03
	RCF-4	P	55.11	0.008	56.86	0.058	7.29	3.47
		N	48.60	0.007	62.96	0.049	6.67	3.22
		O	51.86	0.008	59.91	0.05	6.98	3.35

P: Positive direction, **N:** Negative direction, **O:** Average, **M_y:** Yield moment (kN.m), **M_u:** Ultimate moment (kN.m), **$Ø_y$:** Curvature corresponding to yield moment (1/m), **$Ø_u$:** Curvature corresponding to ultimate moment (1/m), **$\mu_ø$:** Curvature-based ductility ratio, **E_u:** Energy dissipation capacity (kN/m^2).

As the corrosion ratio increased, the yield moments (M_y), ultimate moments and curvature values corresponding to these moment values of reinforced concrete frames also decreased. Considering the curvature-based ductility values, it is observed that there is an increase in ductility values as the corrosion rate increases. This misconception is caused by the corrosion mechanism and the deterioration of the mechanical properties of the reinforcement and the early yielding of the section. According to the energy absorption capacitys values obtained by summing the areas under the cyclic graphs, compared to the reference specimens, RCF_1, RCF_2, RCF_3 and RCF_4 specimens are respectively 10.67%, 16.69%, 20.75% and 25.95% for the positive direction and 11.06%, 11.85%, 20.45% for the negative direction and it is seen that it decreased by 33.89%.

Table 7. Comparison of numerical and experimental results

Specimens	Loading Direction	M_r exp. (kN.m)	M_r num. (kN.m) Right	Exp/Num	M_r exp. (kN.m)	M_r num. (kN.m) Left	Exp/Num
RCF_R	P						
	N	91.80	99.77	0.92	91.80	99.77	0.92
	O						
RCF_1	P	84.98	93.35	0.91	84.98	93.17	0.91
	N	92.66	93.87	0.99	92.66	92.32	1.00
	O	88.82	93.61	0.95	88.82	92.75	0.96
RCF_2	P	83.41	93.69	0.89	83.41	94.23	0.89
	N	99.41	93.32	1.07	99.41	91.54	1.09
	O	91.41	93.51	0.98	91.41	92.89	0.99

Table 7. Comparison of numerical and experimental results (continued)

	P	72.26	82.52	0.88	72.26	81.83	0.88
RCF_3	N	85.41	81.48	1.05	85.41	84.40	1.01
	O	78.84	82.00	0.96	78.84	83.12	0.95
	P	63.20	78.99	0.80	63.20	70.91	0.89
RCF_4	N	73.06	73.48	0.99	73.06	73.60	0.99
	O	68.13	76.24	0.90	68.13	72.26	0.94

P: Positive direction, **N:** Negative direction, **O:** Average,

In Table 7, the calculated numerical and measured experimental moment-carrying capacities of reinforced concrete frames are compared. As seen in Table 7, as the corrosion level increases, the moment carrying capacities of the samples decrease significantly (For example, the RCF_4 sample decreased by 25.78% compared to the RCF_R specimen). Considering the right and left columns of reinforced concrete frames, the bearing capacity capacities for both columns are similar due to the close corrosion levels. The moment values obtained from the analytical study can predict the moment values obtained from the experimental study with a rate of over 89%. As the corrosion ratio increases, deterioration in concrete and reinforcement brings about a decrease in the axial load value. This situation is thought to cause the experimental and analytical moment carrying capacity prediction results for the RCF_4 specimen, which has the highest corrosion ratio, to be at lower levels than the other samples.

CONCLUSION

Differences were observed in moment carrying capacity depending on the corrosion level distributions in the positive and negative loading directions. As the corrosion ratio increases, the cycles become narrower and their energy dissipation capacity decreases. Inconsistent results were obtained between the curvature-based ductility values obtained as a result of the sectional analyzes of corroded specimens. In this context, calculating the ductility ratio of elements exposed to corrosion with energy-based methods will produce more accurate results in evaluations in terms of ductility. In light of the data obtained from sectional analysis, considering reinforcement corrosion in reinforced concrete frames and deteriorations in the mechanical properties of concrete and reinforcement materials, can accurately estimate the moment-carrying capacity of corroded specimens.

ACKNOWLEDGEMENTS

This study was financed by the Scientific Research Projects Commissions of Inonu University under grant number FBA-2021-2483.

Conflict of Interest

The article authors declare that there is no conflict of interest between them.

Author's Contributions

The authors declare that they have contributed equally to the article.

REFERENCES

ABYYHY., (1975). "Afet Bölgelerinde Yapılacak Binalar Hakkında Yönetmelik". Bayındırlık ve İskân Bakanlığı, Ankara, Türkiye.

ABYYHY., (1998). "Afet Bölgelerinde Yapılacak Binalar Hakkında Yönetmelik". Bayındırlık ve İskân Bakanlığı, Ankara, Türkiye.

Akiyama, M., Frangopol, D. M., Arai, M., & Koshimura, S. (2013). Reliability of bridges under tsunami hazards: Emphasis on the 2011 Tohoku-oki earthquake. *Earthquake Spectra*, 29(1), 295-314.

Standard, A. S. T. M. (2003). G1-03. Standard Practice for preparing, cleaning, and evaluating corrosion test specimens, *Annual Book of ASTM Standards*, 3, 17-25.

Binici, H. (2007). March 12 and June 6, 2005 Bingol–Karliova earthquakes and the damages caused by the material quality and low workmanship in the recent earthquakes. *Engineering Failure Analysis*, 14(1), 233-238.

Çağatay, İ. H. (2005). Experimental evaluation of buildings damaged in recent earthquakes in Turkey. *Engineering Failure Analysis*, 12(3), 440-452.

Caglar, N., Demir, A., Ozturk, H., & Akkaya, A. (2015). A simple formulation for effective flexural stiffness of circular reinforced concrete columns. *Engineering Applications of Artificial Intelligence*, 38, 79-87.

Cape, M., Residual service-life assessment of existing R/C structures, MS thesis, Chalmers University of Technology and Milan University of Technology, 1999.

Celik, A., Yalciner, H., Kumbasaroglu, A., & Turan, A. İ. (2022). An experimental study on seismic performance levels of highly corroded reinforced concrete columns. *Structural Concrete*, 23(1), 32-50.

Cheng, X., Ji, X., Henry, R. S., & Xu, M. (2019). Coupled axial tension-flexure behavior of slender reinforced concrete walls. *Engineering Structures*, 188, 261-276.

Dok, G., Ozturk, H., & Demir, A. (2017). Determining moment-curvature relationship of reinforced concrete columns. *The Eurasia Proceedings of Science, Technology, Engineering and Mathematics (EPSTEM)*, 1, 52-58.

Erdik, M., Yüzügüllü, Ö., Yilmaz, C., & Akkas, N. (1992). 13 March, 1992 (Ms= 6· 8) Erzincan earthquake: A preliminary reconnaissance report. *Soil Dynamics and Earthquake Engineering*, 11(5), 279-310.

Applied Technology Council, Mid-America Earthquake Center, Multidisciplinary Center for Earthquake Engineering Research (US), Pacific Earthquake Engineering Research Center, & National Earthquake Hazards Reduction Program (US). (2007). *Interim testing protocols for determining the seismic performance characteristics of structural and nonstructural components*. Federal Emergency Management Agency.

Kaplan, H., Yilmaz, S., Binici, H., Yazar, E., & Çetinkaya, N. (2004). May 1, 2003 Turkey—Bingöl earthquake: damage in reinforced concrete structures. *Engineering Failure Analysis*, 11(3), 279-291.

Lockner, D., Naka, H., Tanaka, H., Ito, H., & Ikeda, R. (2000). Permeability and strength of core samples from the Nojima fault of the 1995 Kobe earthquake. *In Proceedings of the international workshop on the Nojima fault core and borehole data analysis* (Vol. 129, pp. 147-152).

Mondal, G., & Rai, D. C. (2008). Performance of harbour structures in Andaman Islands during 2004 Sumatra earthquake. *Engineering Structures*, 30(1), 174-182.

Sengel, H. S., & Dogan, M. (2013). Failure of buildings during sultandagi earthquake. *Engineering Failure Analysis*, 35, 1-15.

Sheikh, M. N., Tsang, H. H., McCarthy, T. J., Lam, N. T. K. (2010). Yield curvature for seismic design of circular reinforced concrete columns, *Magazine of Concrete Research*, 62(10), 741-748.

TBEC- 2018. Turkish building earthquake code specifications for design of buildings under seismic effects. *Ministry of Disaster and Emergency Management Presidency*, Ankara, Turkey.

Tezcan, S. S., & Ipek, M. (1996). A reconnaissance report: 1995 Dinar, Turkey, earthquake. *Engineering structures*, 18(12), 906-916.

TS 500, (2000). Requirements for design and construction of reinforced concrete structures, turkish standards institute, Ankara, Turkey.

Vecchio, F. J., & Collins, M. P. (1986). The modified compression-field theory for reinforced concrete elements subjected to shear. *ACI J*, 83(2), 219-231.

Wang, X. H., & Liu, X. L. (2008). Modeling the flexural carrying capacity of corroded RC beam. Journal of Shanghai Jiaotong University (Science), 13, 129-135.

Wastı, S. T., Sucuoğlu, H., & Utku, M. (2001). Buildings after the 1 October 1995. *Journal of Earthquake Engineering*, 5(2), 131-151.

XTRACT. v.3.0.8. (2007). Cross-sectional structural αnalysis of components. *Imbsen Software System*. 9912 Business Park Drive, Suite 130, Sacramento CA 95827.

Yalciner, H., & Kumbasaroglu, A. (2020). Experimental evaluation and modeling of corroded reinforced concrete columns. *ACI Structural Journal*, (4).

Yalciner, H., & Kumbasaroglu, A. (2022). Experimental study to predict bond-slip behavior of corroded reinforced concrete columns. *ACI Structural Journal*, 119(5).

Yalciner, H., Kumbasaroglu, A., & Karimi, A. (2019). Prediction of seismic performance levels of corroded reinforced concrete columns as a function of crack width. *Advances in Civil Engineering Materials*, 8(3), 376-397.

Yalciner, H., Kumbasaroglu, A., & Turan, A. İ. (2019). Torsional behavior of reinforced concrete beams with corroded reinforcement. *Structures*, 20, 476-488.

Yalciner, H., Kumbasaroglu, A., El-Sayed, A. K., Balkıs, A. P., Dogru, E., Turan, A. I., & Bicer, K. (2020). Flexural strength of corroded reinforced concrete beams. *ACI Structural Journal*, 117(1).

Wu, Q., & Yuan, Y. S. (2008). Experimental study on the deterioration of mechanical properties of corroded steel bars. *China civil engineering journal*, *41*(12), 42-47.

Yüksel, B., Foroughi, S. (2020). Analysis of bending moment-curvature and the damage limits of reinforced concrete circular columns. *Avrupa Bilim ve Teknoloji Dergisi*, (19), 891-903.

Zhang, M., Liu, R., Li, Y., & Zhao, G. (2018). Seismic performance of a corroded reinforce concrete frame structure using pushover method. *Advances in Civil Engineering*, 2018, 1-12.